Effects of mixing conditions and activator anionic species on the rheology of silicate-activated slag concrete

Sun, Yubo; Mohan, Manu K.; Dai, Xiaodi; Zhang, Yiyuan; Ye, Guang; De Schutter, Geert

DOI
10.1016/j.cemconcomp.2024.105556

Publication date
2024

Document Version
Final published version

Published in
Cement and Concrete Composites

Cement and Concrete Composites 150 (2024) 105556

Contents lists available at ScienceDirect

Cement and Concrete Composites

journal homepage: www.elsevier.com/locate/cemconcomp

Effects of mixing conditions and activator anionic species on the rheology of silicate-activated slag concrete

Yubo Sun [a], Manu K. Mohan [a], Xiaodi Dai [a], Yiyuan Zhang [a], Guang Ye [a,b], Geert De Schutter [a,*]

[a] Magnel-Vandepitte Laboratory, Department of Structural Engineering and Building Materials, Ghent University, 9052, Ghent, Belgium
[b] Microlab, Section of Materials and Environment, Faculty of Civil Engineering and Geosciences, Delft University of Technology, Stevinweg 1, 2628 CN, Delft, the Netherlands

ARTICLE INFO

Keywords:
Alkali-activated slag concrete
Rheology
Microstructure
Reaction kinetics
Reaction products

ABSTRACT

The proper control of the rheological performance of silicate-based alkali-activated slag (AAS) mixtures is problematic, as the conventional superplasticizers become less effective in alkaline media. Nevertheless, several methods have been proposed to improve the workability of silicate-activated AAS, such as by extending the mixing time, and replacing sodium silicate with sodium carbonate activators. However, the underlying fluidizing mechanism is not yet well understood in the literature, which is crucial knowledge to achieve proper rheology control of silicate-activated AAS.

In this study, the effects of mixing conditions and activator anionic species on the rheology of silicate-activated AAS concrete have been assessed. The reaction products, particle size and interparticle interactions, as well as the reaction kinetics in AAS, have been further investigated to understand the distinct fluidizing mechanisms. By using a longer mixing time, it was found that the solid particles formed at early ages are broken down into smaller particles, accompanied by a slight increase in the amount of reaction products to improve the fluidity. With the sodium carbonate substitution, the calcium ions dissolved from slag particles are entrapped into calcium carbonate precipitates to slow down the accumulation of C-(A)-S-H phases, leading to a better dynamic flow. However, the interparticle interactions are intensified due to the formation of larger particles and the declined dispersing effect induced by silicate activators.

1. Introduction

According to the latest statistics, construction activities with Portland cement (PC) concrete approximately account for 5 %–8 % of CO_2 emissions and 14 % of global industrial energy consumption [1,2]. This is mainly due to the very high volume of concrete used annually worldwide, while intrinsically concrete performs better than most other construction materials [3]. Nevertheless, regarding the growing market demand for construction materials [4], it is imminent to find green alternatives for PC to achieve net-zero emissions and reach the European Green Deal by 2050 [5,6]. Among the alternative binders for replacing PC [7,8], alkali-activated material (AAM), which is made of various industrial by-products and cleaned waste materials, is regarded as a promising candidate [9–11], even though the alkaline activators may on the other hand induce carbon emission [12,13]. Many previous studies have illustrated the satisfying mechanical properties and chemical resistance of AAMs compared to PC binders [14–16].

Nevertheless, a critical issue appears as the rapid workability loss of alkali-activated slag (AAS) mixtures, in particular with the presence of silicate in activators [17]. Limited setting time and uncontrolled stiffening process have been frequently reported in silicate-activated AAS, challenging the operations during the fresh stage in practical applications [18–20]. Conventional superplasticizers (SPs) developed for PC materials have been reported to be much less- or completely in-effective in AAMs [21] due to the following aspects:

- Instability of the SP molecule structure in activator solutions with high alkalinity [18,22].
- Competitive adsorption between SP and the anionic groups in alkaline activators [23–25].
- Lower affinity of SPs to be adsorbed on precursor particles (surface charging) [26–28].
- Reduced solubility of SPs in alkaline activators [25,29,30].

* Corresponding author.
E-mail address: geert.deschutter@ugent.be (G. De Schutter).

https://doi.org/10.1016/j.cemconcomp.2024.105556
Received 28 September 2023; Received in revised form 21 February 2024; Accepted 19 April 2024
Available online 20 April 2024

Instead of applying chemical admixtures, several methods have been proposed in the literature to optimize the fresh properties of AAMs. It has been reported that applying a longer mixing time is an effective approach to improve the workability of silicate-activated AAS, which might also extend the short setting time [17,18,31,32]. Apart from that, extending the mixing time may also benefit in reducing the drying shrinkage [31], improving the mechanical strength [32,33], and reducing the permeability [34]. Nevertheless, Palacios and Puertas [32] suggested that longer mixing times were not observed to modify the chemical and mineralogical compositions in the reaction products in AAS. Moreover, a few researchers suggested the rapid setting in silicate-activated AAS can be mitigated by manipulating the ion composition, especially by introducing sodium carbonate into the activator phase. Sodium carbonate is also favored over conventional activators due to its lower cost and less environmental impact [11,35]. As the common activators applied in AAMs, the industrial production of sodium silicate and sodium hydroxide are associated with energy-intensive processes (e.g. high temperature, high pressure, and electrolysis, etc.) [12,36,37]. In contrast, sodium carbonate naturally exists and can be easily extracted from trona mining [38,39], which might further reduce the carbon emission of AAMs from the activator phase [40]. Li et al. [41] found out that sodium carbonate in silicate-based activators does not alter the degree of polymerization of silicate ions, and a proper design of ternary sodium carbonate-hydroxide-silicate activator may achieve both a reasonable setting time and a high compressive strength. Lu et al. [42] studied the properties of similar AAS activated by ternary activators, and they concluded that good time-dependent rheological performance is achievable by using a high concentration of carbonate (>25 %) and reducing the silicate modulus (<0.5) due to the retarding effect. However, the underlying fluidizing mechanism of the methods present above is not yet well understood in the literature, which is a piece of crucial knowledge to better control the fresh properties of silicate-activated AAS.

The main objective of this study is to investigate the effect of mixing conditions and activator anionic species on the rheological behavior of silicate-activated AAS. The rheology of AAS concrete was first assessed through stress growth and flow curve tests, and the properties of reaction products and features of particle interactions were further characterized on the paste fraction. The results have illustrated the distinct fluidizing mechanism by using different approaches, and may contribute to better control of the rheology of silicate-activated AAS mixtures in practical applications.

2. Experimental method

2.1. Materials

The blast furnace slag (BFS) used in this study is provided by Ecocem Benelux B.V., with a density of 2890 kg/m^3. The particle size distribution measured by laser diffraction is given in Fig. 1 (a), and the d_{50} is 8.28 μm. The morphology of BFS particles was detected with a scanning electron microscope (SEM, JEOL JSM-IT 800). BFS grains were uniformly stuck on a conductive tape and coated with a thin layer of platinum to improve the conductivity before visualization. The SEM image was taken under the secondary electrons (SE) mode with an accelerating voltage of 10 kV, as shown in Fig. 1 (b). Details of the chemical composition of BFS determined by X-ray fluorescence (XRF) and loss on ignition (LOI) are listed in Table 1.

Sodium hydroxide and sodium silicate were applied as the main activator in this study. Reagent-grade sodium hydroxide anhydrous pearls were provided by Brenntag N.V., and the sodium silicate solution (15 % Na_2O, 30 % SiO_2, and 55 % water) was provided by PQ Corporation. In addition, sodium carbonate (>99.5 anhydrous, provided by VWR Chemicals) was introduced as a substitute alkaline compound to partially replace the sodium silicate in the activator.

2.2. Mixture proportions

Details of AAS concrete mixtures are presented in Table 2. The BFS content was fixed at 400 kg/m^3 among different mixtures. M1 was designed as the reference silicate-activated AAS concrete, with 4 % Na_2O by the mass of slag and a silicate modulus (molar ratio between SiO_2 and Na_2O) of 1 in the activator. Among all mixtures, the Na_2O content (by the mass of precursors) and water to binder (w/b) ratio were fixed at 4 % and 0.4, respectively, to ensure an identical alkali cation (Na^+) concentration (Note: binder refers to the sum of precursor and solid activators). M2 and M3 were designed with the same composition as M1 to study the influence of mixing conditions on the rheological properties, as shown in Fig. 2. In view of the rapid setting by using sodium silicate activators, M4 and M5 were designed with ternary anionic species to partially replace the silicate content. By keeping a constant 4 % nominal Na_2O concentration in activators, 10 % and 30 % sodium silicate were replaced by an equivalent amount of sodium carbonate in M4 and M5, respectively. As a consequence, the molar ratio between SiO_2 and Na_2O in the activator was slightly decreased. Activators were prepared by dissolving sodium hydroxide, sodium carbonate, and sodium silicate solution (indicated in Table 2) in tap water and cooled down to room temperature 24 h before mixing. Activator solutions obtained were sealed in plastic buckets to prevent moisture evaporation. The aggregate packing in AAS concretes was designed to reach between A16 and B16 curves as indicated in DIN 1045-2.

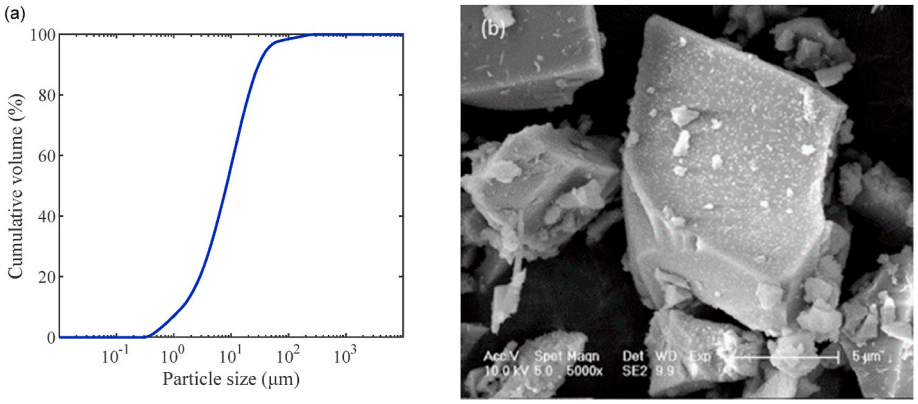

Fig. 1. Physical properties of BFS (a) Particle size distribution; (b) Morphology by SEM (5000 × magnification).

Table 1
Chemical composition of BFS measured by XRF and LOI (mass %).

Precursor	CaO	SiO_2	Al_2O_3	MgO	SO_3	TiO_2	K_2O	Fe_2O_3	MnO	ZrO_2	Other	LOI[a]
BFS	40.9	31.1	13.7	9.16	2.31	1.26	0.69	0.40	0.31	0.12	0.05	0.10

[a] LOI measured by TG analysis at 950 °C.

Table 2
Mixture proportions of AAS concretes used in this study.

Mix	BFS (kg/m^3)	Activator[a]							Aggregate (kg/m^3)[b]			Mixing time (min)
		NaOH (kg/m^3)	Sodium silicate (kg/m^3)	Na_2CO_3 (kg/m^3)	Extra water (kg/m^3)	pH[c]	Molar ratio		0–4 mm	2–8 mm	8–16 mm	
							SiO_2/Na_2O	CO_2/Na_2O				
M1	400	10.32	53.33	–	144.40	13.45	1	0	711	489	580	3
M2	400	10.32	53.33	–	144.40	13.45	1	0	711	489	580	5
M3	400	10.32	53,33	–	144.40	13.45	1	0	711	489	580	10
M4	400	10.32	48.00	1.37	146.92	13.41	0.9	0.4	711	489	580	3
M5	400	10.32	37.33	4.10	151.96	13.32	0.7	1.1	711	489	580	3

[a] Activators are designed with a constant nominal Na_2O content, i.e. 4 % by the mass of BFS.
[b] Aggregate packing is designed to reach between A16 and B16 curves indicated in DIN 1045-2.
[c] Determined by Extech PH150 pH-meter at 20 ± 0.5 °C.

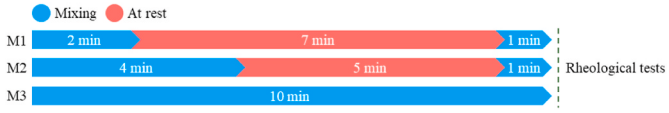

Fig. 2. Mixing protocol used for M1, M2, and M3 in this study.

2.3. Testing program

2.3.1. Preparation of AAS concrete

AAS concrete mixtures were prepared in 30 L batches with a planetary mixer. Solid components including the slag and aggregates were first dry blended for 2 min, and then the activator solution was gradually added in 30 s. As illustrated in Fig. 2, an intermediate rest period was applied in M1 and M2 after the initial mixing and finally remixed for 1 min, whereas M3 was continuously mixed for 10 min before further tests. In total, M1 was mixed for 3 min, while M2 and M3 were subjected to 5 and 10 min mixing, respectively. M4 and M5 were prepared by following the same protocol as M1. At 10 min after the wetting of slag, the ready-mixed AAS concretes were collected for rheological tests.

2.3.2. Concrete rheology

Rheological tests on AAS concrete were performed with an ICAR Plus rheometer, which is fitted with a 4-blade vane. The geometry of the rheometer is presented in Fig. 3, where ribs were attached to the container wall to prevent slippage. Fresh AAS concrete after mixing was loaded into the rheometer container. The concrete was remixed in the container with a handheld mixer for 60 s to ensure the same reference state among different samples [43], and then left at rest until the testing age. The rheological results are presented as the average of three measurements in this study.

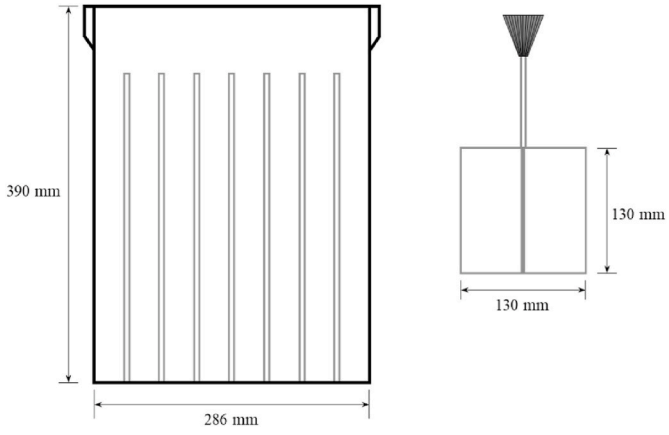

Fig. 3. Geometry of the ICAR Plus rheometer.

Stress growth tests were first conducted at 15 min after the wetting of precursors. By using a constant shear rate of 0.025 rps for 60 s, the torque response first increased to the maximum, and then gradually declined to reach an equilibrium state [44]. The peak torque (T_m) detected along the shear history was converted into the static yield stress (τ_0) according to Eq. (1) [45,46]. Further, the thixotropic behavior of AAS concrete was assessed by the difference between τ_0 and the equilibrium-state shear stress (τ_e) observed after yielding (i.e.: τ_0-τ_e) [34].

$$\tau_0 = \frac{2T_m}{\pi D^3\left(\frac{h}{D}+\frac{1}{3}\right)} \quad (1)$$

where:

τ_0 is the static yield stress (Pa),
T_m is the maximum torque (Nm),
D is the diameter of the vane (m),
h is the height of the vane (m).

Subsequently, flow curve tests were performed on the same batch of concrete. The concrete was first remixed with a handheld mixer for 60 s to eliminate the temporal structural build-up and reach the same reference state among different samples [43]. As shown in Fig. 4, after a pre-shear at 0.6 rps for 60 s, stepwise ascending and descending shear rates were then applied varying between 0.05 and 0.6 rps. Each shear step was conducted for 30 s, and the average torque of the last 10 s was recorded to ensure an equilibrium state. Downward portions of the torque-rotational speed relationships were fitted with the non-linear Herschel-Bulkley model [47] to obtain the flow curves. The dynamic rheological parameters were calculated by the extension of Reiner-Riwlin equations for the Herschel-Bulkley model [48].

2.3.3. Preparation of AAS paste

To better understand the rheological performance of AAS concretes,

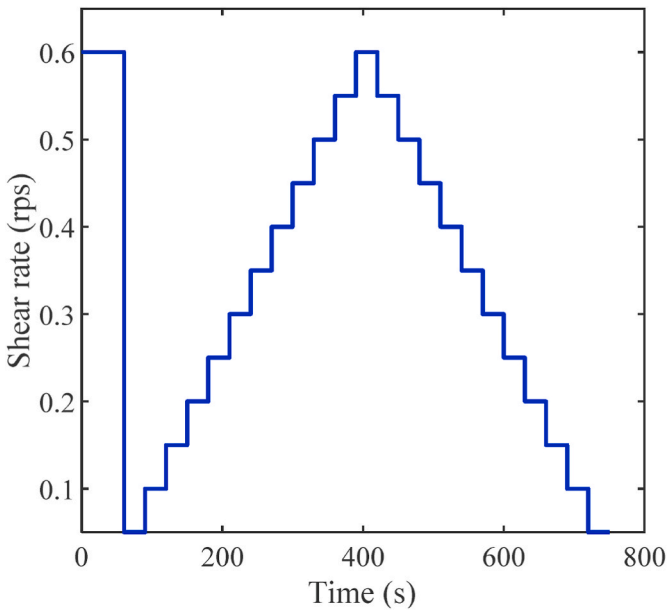

Fig. 4. Shear protocol used for flow curve tests.

the early reaction products and viscoelastic behavior were further investigated on the equivalent paste fraction as illustrated in Table 2. AAS pastes were prepared by mixing 300 g of slag and corresponding activators in a Hobart mixture by following the protocol shown in Fig. 2.

2.3.4. Particle size distribution

By following an identical dispersing approach, the particle size characteristics in the bulk solid fraction of early-age AAS mixtures were analyzed with a laser diffractometer. In specific, 2 ± 0.1 g of the fresh AAS paste after mixing was immediately intermixed with 500 mL isopropanol to arrest the activation reaction [17]. Electromagnetic stirring was applied at 300 rpm for 5 min, followed by an ultrasonic bath treatment for 10 min to disperse and stabilize the solid particles and agglomerates formed in the fresh paste [49,50]. The size distribution of solid particles/agglomerates dispersed in the isopropanol was then measured with laser diffraction. Results present in this study were taken as the mean value of five measurements.

2.3.5. Thermogravimetric analysis (TGA)

The activation reaction in fresh AAS pastes was arrested by using a solvent replacement treatment with water and isopropanol [17], which was immediately done after the mixing progress was finished. Solid residues collected from filtration (with a 0.45 μm filter paper) were vacuum dried (in a ventilated oven at 40 °C for about 5 min) and further ground to pass a 63 μm sieve for characterization, samples were then stored in a sealed bottle inside a vacuum chamber until testing [51].

Thermogravimetric analysis (TGA) was performed on the solid fraction to quantify the early reaction products in AAS. In specific, about 50 mg of the solid powder was loaded into an aluminum oxide (Al_2O_3) crucible, and the sample was incinerated in an argon atmosphere from 40 to 900 °C with a heating rate of 10 °C/min. The mass evolution was recorded as a function of temperature. TGA tests in this study were performed twice to check the repeatability.

2.3.6. Small amplitude oscillation shear (SAOS) test

The particle interaction and viscoelastic features in the early-age AAS paste were then assessed through small amplitude oscillation shear (SAOS) tests with an Anton Paar MCR 102 rheometer (fitted with a 6-blade vane, 22 mm in diameter, and 16 mm in height). The fresh paste after mixing was loaded into a cylindrical cup (27.6 mm inner diameter and 75 mm depth), and the measurement was conducted at 20 ± 0.5 °C with a water bath system. A strain sweep from 0.001 % to 50 % was first conducted with a frequency of 1 Hz to determine the linear viscoelastic domain (LVED) [52–54]. Subsequently, the time sweep was carried out to monitor the structural build-up history in AAS paste. Time sweep measurements were performed at 15 min after the wetting of precursors with a constant strain amplitude of 0.005 % (within the LVED) at 1 Hz for 30 min or the capacity of the rheometer was reached. Storage and loss modulus (G' and G'') were recorded as a function of time along the time sweep. In a cementitious paste, G' refers to the elasticity developed (structural build-up) in the fresh material, which is proportional to the stored energy under excitation [55]. Meanwhile, the energy dissipated due to the viscous behavior is reflected by G''. The loss factor is defined as the ratio between loss and storage modulus (G''/G'), indicating the phase lag between viscous and elastic responses. It has been suggested in cementitious materials that a loss factor of 0 represents a pure elastic behavior, which reveals the formation of a percolating network [56]. For each mixture, the SAOS test was performed on three replicate samples to ensure repeatability, and the curve most close to the average of three measurements is presented.

2.3.7. Calorimetry

The exothermic behavior in AAS pastes along the reaction process was detected with a TAMAIR isothermal calorimeter. For each test, 14 ± 0.01 g of the paste after mixing was loaded into a glass ampoule, which was subsequently sealed and transferred into isothermal channels of the calorimeter. The exothermic process was then continuously recorded at 20 ± 0.5 °C for 100 h. Quartz sand was applied as an inert reference with a specific heat flow of 0.71 J/(g.K). The heat flow of AAS paste is represented as the difference between the sample and reference [57], and results are normalized into 1 g of solid binder (including precursor and solid activators). Due to the thermal disturbance while inserting the glass ampoule, the heat flow recorded at the first 30 min is not compared among different samples. Calorimetry tests were performed twice to check the repeatability.

3. Results and discussion

3.1. Rheology of AAS concrete

3.1.1. Stress growth test

Results of stress growth tests are presented in Table 3. Compared to the reference mixture M1, the static yield stress of M2 and M3 with a longer mixing time was reduced by 30 % and 48 %, respectively. Meanwhile, the degree of thixotropy also significantly declined in M2 and M3. It is indicated that the structuration in fresh AAS concrete was extensively broken down with the extra shear energy applied. In the meantime, the inclusion of sodium carbonate in the activator has led to different results. By replacing sodium silicate with sodium carbonate, the static yield stress first declined by 44 % in M4 but later increased by 8 % in M5 with a higher replacement ratio, as compared to M1. Similar trends were detected in the thixotropic behavior of AAS concrete, and this will be further illustrated in 3.3.

3.1.2. Flow curve test

Hysteresis loops obtained from flow curve tests are plotted in Fig. 5. It is interesting to notice in several mixtures that the ascending and descending flow curves crossed over each other in low shear-rate regions. The most significant overlap was detected in M3 at around a

Table 3
Rheological parameters determined from the stress growth test.

	M1	M2	M3	M4	M5
Static yield stress (Pa)	1358.1	1016.3	796.3	752.9	1464.1
Equilibrium shear stress (Pa)	813.7	566.6	422.1	459.8	854.0
Degree of thixotropy (Pa)	544.5	449.7	374.3	293.2	610.2

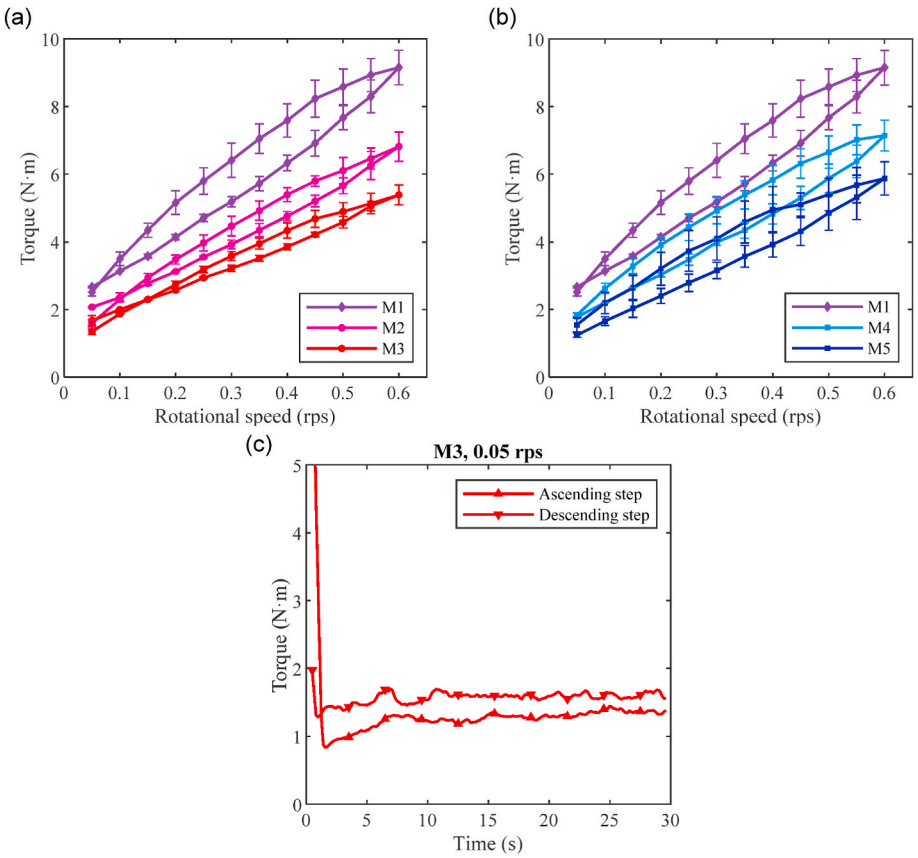

Fig. 5. Results of flow curve tests on different AAS concretes (a) By using different mixing protocols (M1, M2, and M3); (b) By using different activator anionic species in the activator (M1, M4, and M5); (c) Ascending and descending shear steps at 0.05 rps in M3.

higher shear rate of 0.15 rps. Looking into the torque evolution in M3 by applying the lowest shear rate (0.05 rps), as shown in Fig. 5 (c), both steps in ascending and descending phases have reached an equilibrium state in the last 10 s where the data was collected. However, the system maintained a higher energy level in the descending step that a greater torque value compared to the ascending step was observed while reaching the equilibrium state. This might be ascribed to the high early reactivity in silicate-activated AAS mixtures [17,58]. In other words, the accumulation of early reaction products during the period when the flow curve test was conducted has significantly intensified the interparticle interactions in the system, thereby a higher torque is required to maintain the equilibrium flow in descending phases. Accordingly, the difference between the equilibrium torque of ascending and descending shear steps is accounted for by the contribution of both the structural breakdown and accumulation of reaction products while performing the flow curve test.

As is known that the hysteresis loop area between ascending and descending flow curves is a common approach to evaluating the thixotropic behavior of fresh cementitious mixtures. However, the results obtained here indicate that the structural breakdown might be shaded by the rapid accumulation of early reaction products in silicate-activated AAS mixtures, leading to an underestimation of the degree of thixotropy. With a higher ratio of sodium carbonate in the activator, the overlap between ascending and descending curves was gradually mitigated (Fig. 5 (b)), and eventually disappeared in M5. The results illustrate that the accumulation of early reaction products at this stage was considerably decelerated by replacing sodium silicate with sodium carbonate activators.

Dynamic rheological parameters derived by fitting downward portions of flow curves are summarized in Table 4. By extending the mixing time, lower dynamic rheological parameters have been detected in M2 and M3 compared to the reference mix. In the meantime, both dynamic yield stress and consistency factor significantly declined by using sodium carbonate activators in M4 and M5. Moreover, all AAS concretes exhibited shear thickening as indicated by the flow index (>1) with the Herschel-Bulkley model [47]. The shear thickening occurs in fresh cementitious materials as hydrodynamic forces overcome the interparticle repulsion to form clusters in a dynamic flow [59,60]. Consequently, the particles dispersed in the system are temporarily assembled in clusters, and they are free to join and leave depending on flow conditions [61]. With a high shear rate, repulsive forces cannot relax the interparticle contacts in time under the external shear applied [62,63]. In that case, more particles remain in the cluster to accumulate, which blocks the flow path along the shear direction, leading to stronger interparticle collisions and an increase in apparent viscosity [64]. In the case of silicate-activated AAS mixtures, the viscous nature of silicate activators may assist in entrapping more free particles in the cluster while flowing [65], resulting in obvious shear thickening. Moreover, as indicated in earlier paragraphs, the rapid accumulation of early reaction products during the period of flow curve test was conducted may also intensify the shear thickening behavior. At low shear rate regions, a higher torque was required to maintain the equilibrium flow with the increase in time in the descending portion of flow curves, leading to a

Table 4
Rheological parameters determined from the flow curve test.

	M1	M2	M3	M4	M5
Dynamic yield stress (Pa)	377.6	290.5	235.0	284.3	164.3
Consistency factor (Pa·s^n)	139.0	104.3	92.7	122.9	115.8
Flow index (−)	1.29	1.27	1.20	1.23	1.18
R^2	0.9986	0.999	0.9989	0.9981	0.9985

higher apparent viscosity at these lower shear rates and thereby contribute to the shear thickening. It is noteworthy that either a longer mixing time or the substitution with sodium carbonate activator has resulted in a less pronounced shear thickening behavior.

3.2. Investigation on the paste level

3.2.1. Particle size distribution

The size distribution of solid particles/agglomerates in early-age AAS by following the same dispersing approach is presented in Fig. 6. Compared to the starting slag, the size of solid particles significantly increased at the time of 10 min, revealing a strong early-stage agglomeration and accumulation of reaction products in AAS.

By extending the mixing time, it is noticed that the peak of solid particle size distribution slightly moved leftwards, accompanied by an increase of finer fractions. It is indicated that the solid particles/agglomerates in the fresh paste were progressively broken down as a consequence of the extra mixing process applied. The finer particles may fill in the interstitial voids to optimize the wet packing, and more free water is released to lubricate the AAS paste [21]. By contrast, the substitution with sodium carbonate activators has in general resulted in an increase of larger particles. This might be ascribed to the variation in the type of reaction products, which will be further illustrated in 3.2.2.

3.2.2. Characterization of early reaction products

The mass evolution of the solid fraction in AAS paste was recorded as a function of temperature along the heating process, as shown in Fig. 7. The most significant peak observed in the differential thermogravimetry (DTG) curves below 200 °C is ascribed to the dehydration of C-(A)-S-H phases formed in early-age AAS [66,67]. Apart from that, no apparent DTG peaks or hump was detected between 200 and 400 °C (referring to the hydrotalcite-like phases [68]) at this stage, which is consistent with those reported in silicate-activated AAS [58,69]. Eventually, the peak detected from 500 to 800 °C is associated with the decomposition of carbonated phases [70].

The mass losses along the heating process of the solid fraction in early-age AAS in different temperature regions are summarized in Table 5. By applying a longer mixing time, it was found that the amount of C-(A)-S-H phases formed slightly increased. It is indicated that a longer mixing time has led to a more thorough contact between the slag particles and the activator, promoting the dissolution process to form more early reaction products. Meanwhile, the carbonated phases could be considered originated from the starting slag samples, and thus no obvious change was detected in M1, M2, and M3. On the other hand, the substitution with sodium carbonate activator has resulted in a significant increase of the carbonated phase, accompanied by the reduction of C-(A)-S-H phases formed. The results illustrate that the reaction products have been varied by partially using carbonate activators, possibly resulting in the variation in particle size distribution, as shown in Fig. 6.

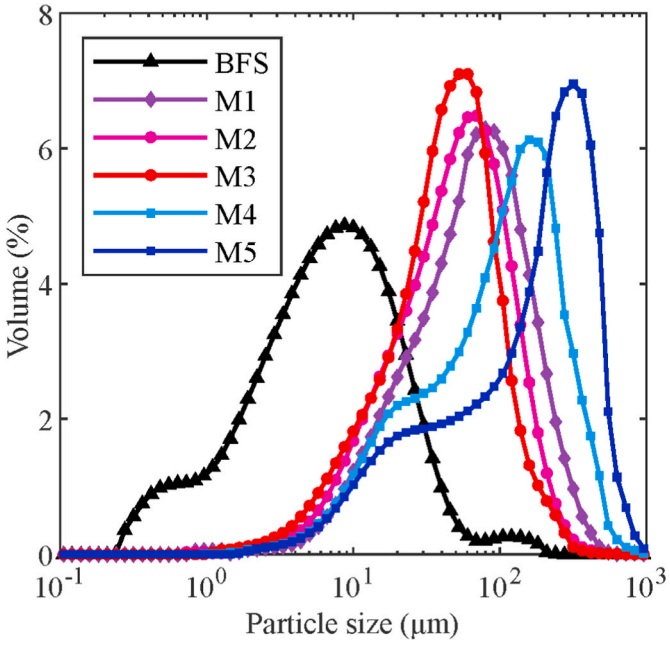

Fig. 6. Particle size distribution of BFS and the solid fraction in AAS pastes.

3.2.3. Small amplitude oscillation shear (SAOS) test

Results of the strain-sweep test among different AAS pastes are presented in Fig. 8. Previous studies have proposed two characteristic peaks of oscillation stress in cementitious materials along with the strain amplitude, referring to the breakage of C–S–H percolations and collapse of colloidal networks in fresh mixtures, respectively [71,72]. Among all AAS pastes, as shown in Fig. 8, it was found that the oscillation stress first increased to a peak value at around 0.2 %, which is associated with the C-(A)-S-H percolations between slag particles [65,73]. After the initial yielding, the oscillation stress slightly declined to a lower level, and further exhibited a steep increase at higher strain regions.

By extending the mixing time (Fig. 8 (a)), the peak of stress ascribed to the C-(A)-S-H percolations gradually turned less pronounced. The results suggest that the interconnection between reaction products was progressively broken down due to the extra shear energy applied, leading to a lower degree of flocculation in the fresh paste. In that case, the water entrapped in the early-age flocs can be released to fluidize the mixture.

Meanwhile, opposite trends have been observed in Fig. 8 (b). The intensity of oscillation stress significantly improved with a higher ratio of sodium carbonate in the activator. It is noteworthy that an obvious subpeak occurred in M5 at around 10 % strain amplitude, which is attributed to the rupture of colloidal interaction networks in a flocculated system [58,72]. This might be correlated to the large particles (Fig. 6) and $CaCO_3$ precipitates (Fig. 7) formed in the system. Previous studies suggested that the presence of CO_3^{2-} anions in AAS preferably incorporated with Ca^{2+} cations dissolved from slag particles to assemble calcium carbonates, and the formation of C-(A)-S-H gels becomes predominant only if the CO_3^{2-} anions present in the pore solution are exhausted [74,75]. As a consequence, $CaCO_3$ precipitations may intensify the interparticle interactions between solid grains, leading to stronger colloidal interactions in the system [76]. In M4 and M5, both C-(A)-S-H percolation and colloidal interaction are intensified compared to M1, which might be also ascribed to the reduced dispersing effect of sodium silicate activators. In silicate-activated AAS, the sodium silicate presents as interstitial gels to hinder the flocculation [73], and the colloidal interaction in turn becomes negligible [65]. With a lower content of silicate species in the activator, such dispersing effect turned less pronounced in the fresh paste, and the colloidal interaction between solid grains was predominant again. Thereby, the collapse of colloidal networks was observed in M5 with higher strain amplitude, accompanied by an intensified C-(A)-S-H percolation.

The evolution of storage modulus and loss factor in AAS pastes are presented in Fig. 9. As shown in Fig. 9 (a), a steep structuration process has been detected in the reference mixture M1 after slow development at the first couple of minutes. It has been revealed that the silicate activators significantly promoted the dissolution of Ca^{2+} cations, leading to the formation of massive C-(A)-S-H gels in silicate-activated AAS [58]. Moreover, silicate species in the pore solution may provide nucleation sites to facilitate the precipitation of early reaction products [77,78]. Thereby, a relatively high storage modulus (450 KPa) was achieved in M1 at the end of the time-sweep measurement.

Further, the increase in mixing time led to only a slight reduction in the degree of build-up over time, and the final storage modulus was reduced by 4.6 % and 9.5 % with the 5-min and 10-min mixing protocol,

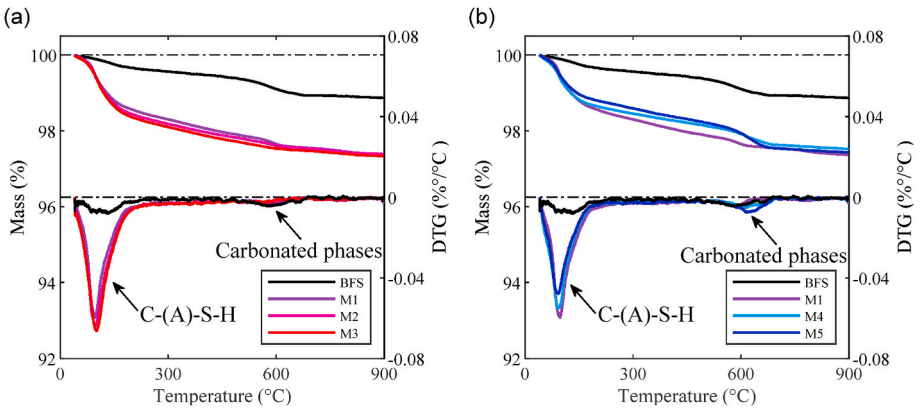

Fig. 7. TG and DTG curves of the solid fraction in early-age AAS (a) By using different mixing method (M1, M2, and M3); (b) By using different activator anionic species in the activator (M1, M4, and M5).

Table 5
The mass losses along the heating process of the solid fraction in early-age AAS.

Mass loss (%)	M1	M2	M3	M4	M5
<200 °C	1.43	1.56	1.62	1.35	1.20
500–800 °C	0.44	0.39	0.43	0.56	0.74

respectively. It is indicated that the structural breakdown induced by the extra shear energy was progressively recovered due to the continuous dissolution and high early-stage reactivity [17]. By contrast, the substitution of sodium silicate with carbonate activators dramatically declined the structuration rate, and merely 54 % storage modulus was achieved in M5 compared to M1 at the end of the measurement. Similar trends have been observed in the viscoelastic behavior of AAS mixtures, as shown in Fig. 9 (b). As the reaction proceeded, the loss factor of M1 gradually declined and almost reached 0 at the end, indicating a nearly elastic behavior with percolated network [56]. In addition, a longer mixing time has led to a slight increase in the loss factor over time, while the mixtures with higher substitution level of carbonate activator exhibited apparently more viscous behaviors.

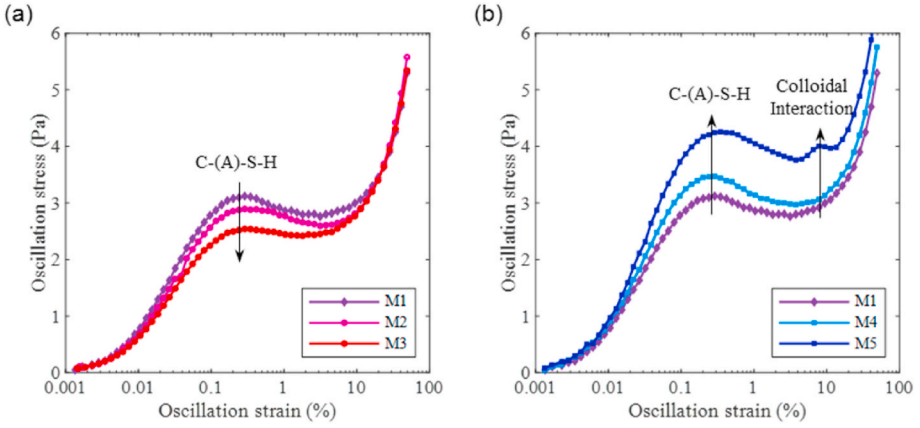

Fig. 8. Oscillation stress as a function of strain amplitude (a) AAS with different mixing conditions; (b) AAS with different anionic activators.

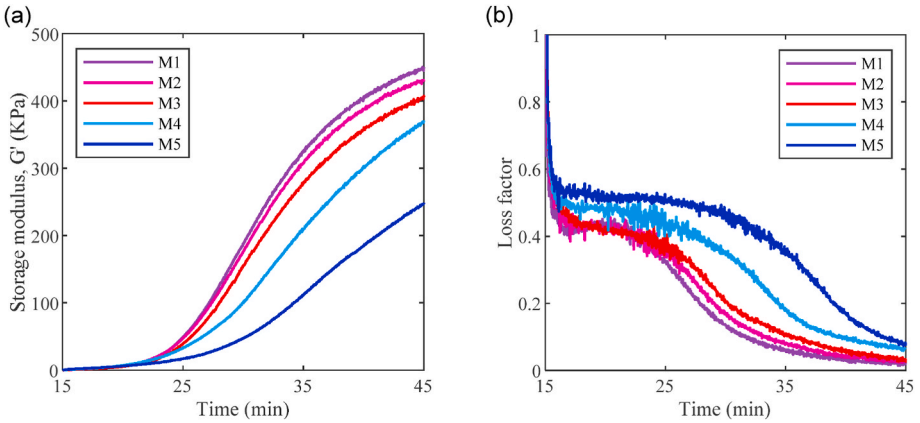

Fig. 9. Evolution of storage modulus and loss factor as a function of time in AAS pastes (a) Storage modulus; (b) Loss factor.

3.2.4. Reaction kinetics

The exothermic characteristics in AAS pastes up to 100 h are illustrated in Fig. 10. No apparent impact on the reaction kinetics was observed by extending the mixing time, as shown in Fig. 10 (a). On the other hand, the intensity of heat flow in AAS pastes was reduced with a higher content of sodium carbonate in the activator. As shown in Fig. 10 (b), the maximum heat flow of acceleration peaks in M4 and M5 decreased by 1.7 % and 6.8 % compared to M1, respectively. This might be attributed to the declined alkalinity in the activator (Table 2), which negatively affected the dissolution of precursor grains. In turn, fewer ions are released from the precursor to contribute to the subsequent reactions, leading to a lower heat flow during the induction and acceleration stage of reactions, as well as a reduction in the cumulative heat release.

In addition, it was observed that the maximum heat flow during acceleration peaks was slightly advanced in M4 and M5 as compared to the reference mixture. A few studies have reported a significant extension of the induction period in AAS by using solely sodium carbonate compared to sodium silicate activators [41,79,80], which is ascribed to its low alkalinity nature. However, Li et al. [41] suggested that the effect of sodium carbonate on the reaction kinetics is negligible in AAS mixtures with a high dose of NaOH, where the early reactivity is predominated by the high alkalinity in the system. The earlier onset of acceleration stage reactions observed in Fig. 10 (b) by applying sodium carbonate could be explained by the mitigation of the retarding effect, which was induced by the silicate species in the activator. A few studies suggested that a high silicate concentration in the activator inhibits the dissolution of silicate species originated from the slag particles [81,82], whereas the other ions are rapidly released into the pore solution of AAS [58]. Thereby, a residual Si-rich layer is formed on the outer slag surface, obstructing further ion exchange [81]. It has been suggested the induction period of silicate-activated AAS is proportional to the silicate in the activator to be consumed up, and the acceleration stage reaction takes place once the silicate species dissolved from slag particles are incorporated in the reaction products [83,84]. Accordingly, the retarding effect of silicate species was gradually mitigated with the substitution of sodium carbonate, and earlier acceleration peaks have been detected in Fig. 10 (b).

3.3. Discussion and perspective

The results present in this study have illustrated that both a longer mixing time and substitution with sodium carbonate activators could effectively improve the dynamic flow of silicate-activated AAS concrete, in terms of lower yield stress and viscosity. No apparent modifications were detected in calorimetry results before the acceleration stage reactions, which suggests that both methods have almost negligible influence on the early-stage reaction kinetics to affect the rheological properties of AAS. Nevertheless, the fluidizing effects could be attributed to their distinct effects on the variation of the type and amount of reaction products, as well as the interparticle interactions.

By extending the mixing time, solid particles and agglomerates formed in the early-age AAS were progressively broken down into smaller particles (Fig. 6), and the water entrapped in agglomerates are released to improve the fluidity of the mixture. This is also reflected by the declined peak oscillation stress along the strain amplitude (Fig. 8), revealing a lower degree of interparticle C-(A)-S-H percolation. In addition, longer mixing time also led to a slight increase in the amount of C-(A)-S-H phases formed, as revealed by the TGA result (Fig. 7). As a consequence, the interparticle voids in AAS are more filled with the finer particles, leading to a better fluidity [21] and a higher mechanical strength in the hardened stage [32]. However, due to the extensive structural breakdown, a longer mixing time has resulted in a slight deceleration in the subsequent structural build-up (Fig. 9).

On the other hand, the fluidizing effect of substitution with sodium carbonate in silicate-activated AAS is attributed to the modification of the reaction progress and reaction products. First of all, as shown in Table 2, a higher sodium carbonate content in the activator has led to the reduction of alkalinity, decelerating the initial dissolution and early-stage activation reactions. In addition, the Ca^{2+} cations dissolved in the pore solution are more incorporated with carbonate anions to precipitate into $CaCO_3$ phases at early ages, which is supported by the intensified peak correlated to the carbonated phases in DTG curves (Fig. 7). Due to the declined availability of Ca^{2+} cations, the C-(A)-S-H phases, as the primary early reaction products in AAS [17], were less accumulated at this stage. This is also reflected by the reduction of peaks representing C-(A)-S-H phases in DTG curves (Fig. 7). Thereby, the subsequent structuration progress was significantly decelerated, accompanied by a more viscous behavior (Fig. 9), leading to more fluid AAS mixtures.

Finally, the results of stress growth tests reveal that M1 and M5 showed higher yield stress and degree of thixotropy in the static state than other mixtures. It has been proposed in the literature that the thixotropic behavior of cementitious materials is a combined effect of colloidal interactions and chemical reactions [85]. The high static state response detected in M5 could be ascribed to the former case. Larger particles and agglomerates were detected in M5 with the substitution of sodium carbonate activators (Fig. 6), resulting in a stronger colloidal interaction and thixotropic behavior in the system, as indicated by the secondary oscillation stress peak observed in M5 (Fig. 8). By contrast, the chemical reaction progress is more predominant in M1, and the rapid accumulation of C-(A)-S-H phases has resulted in the thixotropic build-up in a silicate-activated AAS. M4 in turn exhibited lower static-state responses than M1 and M5 due to the compensation between

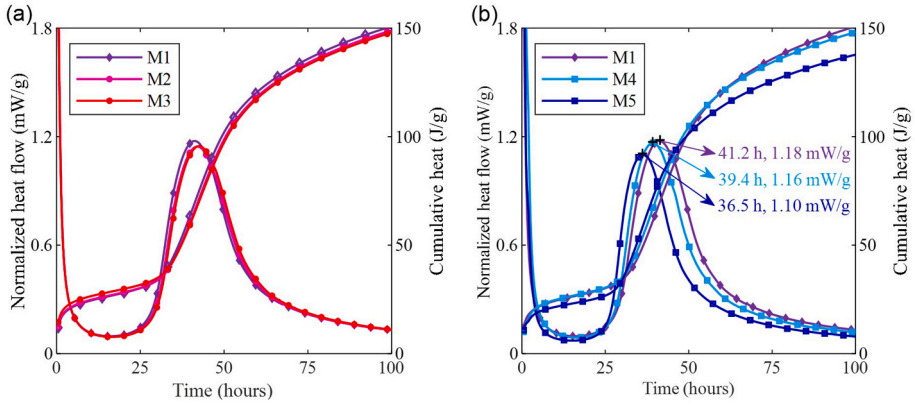

Fig. 10. Calorimetry results of AAS pastes (a) AAS with different mixing conditions; (b) AAS with different anionic activators (Please note, results are normalized into 1 g of solid binder, including precursor and solid activators).

colloidal interactions and chemical reactions. After the broken down of colloidal network by using high shear rate in the flow curve test, lower dynamic rheological parameters have been detected in M5 compared to M1 and M4.

In general, the rheology of silicate-activated AAS progressively deteriorates over time, as a consequence of the rapid accumulation of early reaction products and intensified interparticle interactions. The proper rheology control of silicate-activated AAS concrete remains problematic due to the absence of effective admixtures, obstructing its large-scale applications. As the common practice to improve the workability, substituting sodium silicate with carbonate activators may slow down the accumulation of C-(A)-S-H phases to improve the dynamic flow. However, the interparticle interactions are increased due to the formation of larger particles and the declined silicate activator dispersing effect. In the meantime, a longer mixing time may break down the agglomerates and large particles to improve the fluidity, while the extra production time and cost should be taken into account in practical applications. To achieve proper rheology control, results present indicate that new generations of admixtures dedicated to silicate-activated AAS should be preciously tailored considering both the early reaction rate and interparticle interactions to achieve the best compensation, whereas only the latter has been addressed in the design of conventional SPs used in PC mixtures [86]. A few studies have proposed using retarding admixtures in silicate-activated AAS mixtures to improve the workability by slowing down the early-stage reactions [87–89], while the retarding effect of silicate activators on the induction stage reactions might on the other hand result in a much-delayed setting and very limited first-day strength development [88,90]. Thus, modifications on other factors such as temperature, curing conditions, and additives should also be considered to produce AAS concrete with desirable engineering properties.

4. Conclusions

In this research, a comprehensive study has been done to assess the effect of mixing conditions and activator anionic species on the rheology of AAS concrete. Reaction products, particle size and interparticle interactions, as well as the reaction kinetics in AAS have been further investigated to understand the distinct fluidizing mechanisms by using either approach.

By extending the mixing time from 3 to 5 min, the static and dynamic yield of AAS concrete declined 25 % and 23 %, respectively. This is ascribed to the breakdown of solid particles and agglomerates formed in the early-age AAS. Meanwhile, more reaction products with finer particles in AAS were formed at this stage, which may fill in the interparticle voids to improve the fluidity, and also lead to better mechanical properties in hardened AAS. No significant modification in the reaction kinetics and types of reaction products were detected by extending the mixing time.

The dynamic flow of AAS concrete was significantly improved by replacing sodium silicate activators with an equivalent amount of sodium carbonate activators. Calcium cations dissolved from BFS at early ages were more incorporated with CO_3^{2-} in the activator to precipitate into $CaCO_3$, decelerating the early-stage accumulation of C-(A)-S-H reaction products and the subsequent structuration in AAS. However, the interparticle C-(A)-S-H percolation and colloidal interaction in AAS were progressively intensified with a higher replacement ratio. Increased static yield stress and degree of thixotropy were observed in AAS concrete, due to the formation of larger particles in the system and the declined dispersing effect of silicate activators. Both the early reaction rate and interparticle interactions should be considered to better control the fresh properties of silicate-activated AAS.

CRediT authorship contribution statement

Yubo Sun: Conceptualization, Investigation, Methodology, Writing – original draft. **Manu K. Mohan:** Investigation, Methodology, Writing – original draft. **Xiaodi Dai:** Investigation, Methodology, Writing – original draft. **Yiyuan Zhang:** Investigation, Methodology, Writing – original draft. **Guang Ye:** Supervision, Writing – review & editing. **Geert De Schutter:** Funding acquisition, Supervision, Writing – review & editing.

Declaration of competing interest

The authors declared that we have no conflicts of interest in this work. We declare that we do not have any commercial or associative interest that represents a conflict of interest in connection with the work submitted.

Data availability

Data will be made available on request.

Acknowledgments

This paper presents the research results from the DuRSAAM project. The authors wish to acknowledge the financial support from the European Union's Horizon 2020 research and innovation programme (ETN DuRSAAM – H2020-MSCA-ITN-2018-813596).

References

[1] J.S.J. van Deventer, C.E. White, R.J. Myers, A roadmap for production of cement and concrete with low-CO2 emissions, Waste and Biomass Valorization 12 (2021) 4745–4775.
[2] E. Thwe, D. Khatiwada, A. Gasparatos, Life cycle assessment of a cement plant in Naypyitaw, Myanmar, Clean. Environ. Syst. 2 (2021) 100007.
[3] M.F. Ashby, Materials and the Environment: Eco-Informed Material Choice, Elsevier, 2012.
[4] G. Ellis, Are there any practical alternatives to the manufacture of Portland cement clinker? J. Chin. Ceram. Soc. 40 (2012) 61–68.
[5] I. Tsiropoulos, W. Nijs, D. Tarvydas, P. Ruiz, Towards net-zero emissions in the EU energy system by 2050, Insights from Scenar. Line with 2030 (2020), https://doi.org/10.2760/081488, 2050 Ambitions Eur. Green Deal, JRC Technical Reports.
[6] L.C. Vieira, M. Longo, M. Mura, Are the European manufacturing and energy sectors on track for achieving net-zero emissions in 2050? An empirical analysis, Energy Pol. 156 (2021) 112464.
[7] M.C.G. Juenger, F. Winnefeld, J.L. Provis, J.H. Ideker, Advances in alternative cementitious binders, Cement Concr. Res. 41 (2011) 1232–1243, https://doi.org/10.1016/j.cemconres.2010.11.012.
[8] A. Sivakrishna, A. Adesina, P.O. Awoyera, K.R. Kumar, Green concrete: a review of recent developments, Mater. Today Proc. 27 (2020) 54–58, https://doi.org/10.1016/j.matpr.2019.08.202.
[9] P. Duxson, D.G. Brice, Chemical research and climate change as drivers in the commercial adoption of alkali activated materials, 145–155, https://doi.org/10.1007/s12649-010-9015-9, 2010.
[10] J.L. Provis, Geopolymers and other alkali activated materials: Why, how, and what? Mater. Struct. Constr. 47 (2014) 11–25, https://doi.org/10.1617/s11527-013-0211-5.
[11] P. Krivenko, Why alkaline activation - 60 years of the theory and practice of alkali-activated materials, J. Ceram. Sci. Technol. 8 (2017) 323–333, https://doi.org/10.4416/JCST2017-00042.
[12] M. Fawer, M. Concannon, W. Rieber, Life cycle inventories for the production of sodium silicates, Int. J. Life Cycle Assess. 4 (1999) 207–212.
[13] L.K. Turner, F.G. Collins, Carbon dioxide equivalent (CO2-e) emissions: a comparison between geopolymer and OPC cement concrete, Construct. Build. Mater. 43 (2013) 125–130, https://doi.org/10.1016/j.conbuildmat.2013.01.023.
[14] A. Fernández-Jiménez, J.G. Palomo, F. Puertas, Alkali-activated slag mortars: mechanical strength behaviour, Cement Concr. Res. 29 (1999) 1313–1321, https://doi.org/10.1016/S0008-8846(99)00154-4.
[15] M. Albitar, M.S.M. Ali, P. Visintin, M. Drechsler, Durability evaluation of geopolymer and conventional concretes, Construct. Build. Mater. 136 (2017) 374–385, https://doi.org/10.1016/j.conbuildmat.2017.01.056.
[16] T.A. Aiken, W. Sha, J. Kwasny, M.N. Soutsos, Cement and Concrete Research Resistance of geopolymer and Portland cement based systems to silage ef fl uent attack, Cement Concr. Res. 92 (2017) 56–65, https://doi.org/10.1016/j.cemconres.2016.11.015.
[17] M. Palacios, S. Gismera, M.M. Alonso, J.B. Espinose, D. Lacaillerie, B. Lothenbach, A. Favier, C. Brumaud, F. Puertas, Cement and Concrete Research Early reactivity of sodium silicate-activated slag pastes and its impact on rheological properties,

Cement Concr. Res. 140 (2021) 106302, https://doi.org/10.1016/j.cemconres.2020.106302.
[18] M. Palacios, P.F.G. Banfill, F. Puertas, Rheology and setting of alkali-activated slag pastes and mortars: effect of organic admixture, ACI Mater. J. 105 (2008) 140.
[19] C. Qing-Hua, S.L. Sarkar, A study of rheological and mechanical properties of mixed alkali activated slag pastes, Adv. Cement Base Mater. 1 (1994) 178–184, https://doi.org/10.1016/1065-7355(94)90009-4.
[20] E. Douglas, A. Bilodeau, V.M. Malhotra, Properties and durability of alkali-activated slag concrete, Mater. J. 89 (1992) 509–516.
[21] C. Lu, Z. Zhang, C. Shi, N. Li, D. Jiao, Q. Yuan, Rheology of alkali-activated materials: a review, Cem. Concr. Compos. 121 (2021) 104061, https://doi.org/10.1016/j.cemconcomp.2021.104061.
[22] M. Palacios, F. Puertas, Stability of superplasticizer and shrinkage-reducing admixtures Stability of superplasticizer and shrinkage-reducing admixtures in high basic media, Mater. Construcción 54 (2004) 65–86.
[23] V.B. Jr, P. Hrubý, V. Iliushchenko, M. Kalina, Cement and Concrete Research on the action mechanism of lignosulfonate plasticizer in alkali-activated slag-based system Luk a, 157, https://doi.org/10.1016/j.cemconres.2022.106822, 2022.
[24] D. Marchon, U. Sulser, A. Eberhardt, R.J. Flatt, Molecular design of comb-shaped polycarboxylate dispersants for environmentally friendly concrete, Soft Matter 9 (2013) 10719–10728.
[25] L. Lei, H.K. Chan, Investigation into the molecular design and plasticizing effectiveness of HPEG-based polycarboxylate superplasticizers in alkali-activated slag, Cement Concr. Res. 136 (2020) 106150, https://doi.org/10.1016/j.cemconres.2020.106150.
[26] M. Palacios, Y.F. Houst, P. Bowen, F. Puertas, Adsorption of superplasticizer admixtures on alkali-activated slag pastes, Cement Concr. Res. 39 (2009) 670–677, https://doi.org/10.1016/j.cemconres.2009.05.005.
[27] A. Kashani, J.L. Provis, G.G. Qiao, J.S.J. Van Deventer, The interrelationship between surface chemistry and rheology in alkali activated slag paste, Construct. Build. Mater. 65 (2014) 583–591, https://doi.org/10.1016/j.conbuildmat.2014.04.127.
[28] T. Luukkonen, M. Sarkkinen, K. Kemppainen, J. Rämö, U. Lassi, Applied Clay Science Metakaolin geopolymer characterization and application for ammonium removal from model solutions and land fi ll leachate, Appl. Clay Sci. 119 (2016) 266–276, https://doi.org/10.1016/j.clay.2015.10.027.
[29] T. Conte, J. Plank, Impact of molecular structure and composition of polycarboxylate comb polymers on the flow properties of alkali-activated slag, Cement Concr. Res. 116 (2019) 95–101, https://doi.org/10.1016/j.cemconres.2018.11.014.
[30] C. Paillard, M.A. Cordoba, N. Sanson, J.-B. d'Espinose de Lacaillerie, G. Ducouret, P. Boustingorry, M. Jachiet, C. Giraudeau, V. Kocaba, The role of solvent quality and of competitive adsorption on the efficiency of superplasticizers in alkali-activated slag pastes, Cement Concr. Res. 163 (2023) 107020.
[31] F. Puertas, C. Varga, M.M. Alonso, Rheology of alkali-activated slag pastes. Effect of the nature and concentration of the activating solution, Cem. Concr. Compos. 53 (2014) 279–288, https://doi.org/10.1016/j.cemconcomp.2014.07.012.
[32] M. Palacios, F. Puertas, Effectiveness of mixing time on hardened properties of waterglass-activated slag pastes and mortars, ACI Mater. J. 108 (2011) 73.
[33] A.H. Mahmood, S.J. Foster, A. Castel, Effects of mixing duration on engineering properties of geopolymer concrete, Construct. Build. Mater. 303 (2021) 124449.
[34] F. Puertas, B. González-Fonteboa, I. González-Taboada, M.M. Alonso, M. Torres-Carrasco, G. Rojo, F. Martínez-Abella, Alkali-activated slag concrete: fresh and hardened behaviour, Cem. Concr. Compos. (2018), https://doi.org/10.1016/j.cemconcomp.2017.10.003.
[35] C. Shi, D. Roy, P. Krivenko, Alkali-activated Cements and Concretes, CRC press, 2003.
[36] F. Du, D.M. Warsinger, T.I. Urmi, G.P. Thiel, A. Kumar, J.H. Lienhard V, Sodium hydroxide production from seawater desalination brine: process design and energy efficiency, Environ. Sci. Technol. 52 (2018) 5949–5958.
[37] X. Dai, S. Aydın, M.Y. Yardımcı, K. Lesage, G. De Schutter, Effect of Ca (OH) 2 addition on the engineering properties of sodium sulfate activated slag, Materials 14 (2021) 4266.
[38] S. Ash, Mineral Commodity Summaries 2019, US Geological Survey, Reston, VA, 2019.
[39] A.D. Adesina, Effect of Green Activators on the Properties of Alkali Activated Materials: a Review, vol. 1, RILEM Publ, 2018, pp. 431–436.
[40] A. Adesina, Performance and sustainability overview of sodium carbonate activated slag materials cured at ambient temperature, Resour. Environ. Sustain. 3 (2021) 100016.
[41] N. Li, C. Shi, Z. Zhang, Understanding the roles of activators towards setting and hardening control of alkali-activated slag cement, Composites, Part B 171 (2019) 34–45, https://doi.org/10.1016/j.compositesb.2019.04.024.
[42] C. Lu, Z. Zhang, J. Hu, C. Shi, Cement and Concrete Research Effects of anionic species of activators on the rheological properties and early gel characteristics of alkali-activated slag paste, Cement Concr. Res. 162 (2022) 106968, https://doi.org/10.1016/j.cemconres.2022.106968.
[43] A. Favier, G. Habert, J.B. D'Espinose De Lacaillerie, N. Roussel, Mechanical properties and compositional heterogeneities of fresh geopolymer pastes, Cement Concr. Res. 48 (2013) 9–16, https://doi.org/10.1016/j.cemconres.2013.02.001.
[44] H. Yao, Z. Xie, Z. Li, C. Huang, Q. Yuan, X. Zheng, The relationship between the rheological behavior and interlayer bonding properties of 3D printing cementitious materials with the addition of attapulgite, Construct. Build. Mater. 316 (2022) 125809.
[45] E.P. Koehler, D.W. Fowler, Development of a Portable Rheometer for Fresh Portland Cement Concrete, 2004.
[46] X. Dai, Y. Tao, K. Van Tittelboom, G. De Schutter, Rheological and mechanical properties of 3D printable alkali-activated slag mixtures with addition of nano clay, Cem. Concr. Compos. 139 (2023) 104995.
[47] D. Feys, R. Verhoeven, G. De Schutter, Fresh self compacting concrete, a shear thickening material, Cement Concr. Res. 38 (2008) 920–929, https://doi.org/10.1016/j.cemconres.2008.02.008.
[48] G. Heirman, L. Vandewalle, D. Van Gemert, Ó. Wallevik, Integration approach of the Couette inverse problem of powder type self-compacting concrete in a wide-gap concentric cylinder rheometer, J. Nonnewton. Fluid Mech. 150 (2008) 93–103, https://doi.org/10.1016/j.jnnfm.2007.10.003.
[49] S.S. Potgieter, L. Marjanovic, A further method for chloride analysis of cement and cementitious materials—ICP-OES, Cement Concr. Res. 37 (2007) 1172–1175.
[50] M.R. Rostami, F. Abbassi-Sourki, H. Bouhendi, Synergistic effect of branched polymer/nano silica on the microstructures of cement paste and their rheological behaviors, Construct. Build. Mater. 201 (2019) 159–170.
[51] M.K. Mohan, A.V. Rahul, Y. Tao, G. De Schutter, K. Van Tittelboom, Hydration re-initiation of borated CSA systems with a two-stage mixing process: an application in extrusion-based concrete 3D printing, Cement Concr. Res. 159 (2022) 106870.
[52] Q. Yuan, D. Zhou, K.H. Khayat, D. Feys, C. Shi, On the measurement of evolution of structural build-up of cement paste with time by static yield stress test vs. small amplitude oscillatory shear test, Cement Concr. Res. 99 (2017) 183–189.
[53] X. Dai, S. Aydın, M. Yücel, K. Lesage, G. De Schutter, Cement and Concrete Research Effects of activator properties and GGBFS/FA ratio on the structural build-up and rheology of AAC, Cement Concr. Res. 138 (2020) 106253, https://doi.org/10.1016/j.cemconres.2020.106253.
[54] X. Dai, S. Aydin, M. Yücel, G. De Schutter, Rheology and structural build-up of sodium silicate- and sodium hydroxide-activated GGBFS mixtures, Cem. Concr. Compos. 131 (2022) 104570, https://doi.org/10.1016/j.cemconcomp.2022.104570.
[55] Q. Yuan, X. Lu, K.H. Khayat, D. Feys, C. Shi, Small amplitude oscillatory shear technique to evaluate structural build-up of cement paste, Mater. Struct. 50 (2017) 1–12.
[56] A.M. Mostafa, A. Yahia, New approach to assess build-up of cement-based suspensions, Cement Concr. Res. 85 (2016) 174–182.
[57] L. Wadsö, Operational issues in isothermal calorimetry, Cement Concr. Res. 40 (2010) 1129–1137.
[58] Y. Sun, L. Miranda, D. Lima, L. Rossi, D. Jiao, Z. Li, G. Ye, G. De Schutter, Cement and Concrete Research Interpretation of the early stiffening process in alkali-activated slag pastes, Cement Concr. Res. 167 (2023) 107118, https://doi.org/10.1016/j.cemconres.2023.107118.
[59] B.J. Maranzano, N.J. Wagner, The effects of particle size on reversible shear thickening of concentrated colloidal dispersions, J. Chem. Phys. 114 (2001) 10514–10527.
[60] B.J. Maranzano, N.J. Wagner, The effects of interparticle interactions and particle size on reversible shear thickening: Hard-sphere colloidal dispersions, J. Rheol. (N. Y. N. Y). 45 (2001) 1205–1222.
[61] D. Feys, R. Verhoeven, G. De Schutter, Why is fresh self-compacting concrete shear thickening? Cement Concr. Res. 39 (2009) 510–523, https://doi.org/10.1016/j.cemconres.2009.03.004.
[62] J.R. Melrose, R.C. Ball, "Contact networks" in continuously shear thickening colloids, J. Rheol. (N. Y. N. Y). 48 (2004) 961–978.
[63] J.R. Melrose, R.C. Ball, Continuous shear thickening transitions in model concentrated colloids—the role of interparticle forces, J. Rheol. (N. Y. N. Y). 48 (2004) 937–960.
[64] R.G. Egres, N.J. Wagner, The rheology and microstructure of acicular precipitated calcium carbonate colloidal suspensions through the shear thickening transition, J. Rheol. (N. Y. N. Y). 49 (2005) 719–746.
[65] M.F. Alnahhal, T. Kim, A. Hajimohammadi, Distinctive rheological and temporal viscoelastic behaviour of alkali-activated fly ash/slag pastes: a comparative study with cement paste, Cement Concr. Res. 144 (2021) 106441, https://doi.org/10.1016/j.cemconres.2021.106441.
[66] I. Garcia-Lodeiro, A. Palomo, A. Fernández-Jiménez, D.E. MacPhee, Compatibility studies between N-A-S-H and C-A-S-H gels. Study in the ternary diagram Na2O-CaO-Al2O3-SiO 2-H2O, Cement Concr. Res. 41 (2011) 923–931, https://doi.org/10.1016/j.cemconres.2011.05.006.
[67] E. Kapeluszna, Ł. Kotwica, A. Różycka, Ł. Gołek, Incorporation of Al in CASH gels with various Ca/Si and Al/Si ratio: microstructural and structural characteristics with DTA/TG, XRD, FTIR and TEM analysis, Construct. Build. Mater. 155 (2017) 643–653.
[68] E. Kanezaki, Thermal behavior of the hydrotalcite-like layered structure of Mg and Al-layered double hydroxides with interlayer carbonate by means of in situ powder HTXRD and DTA/TG, Solid State Ionics 106 (1998) 279–284.
[69] S.-D. Wang, K.L. Scrivener, Hydration products of alkali activated slag cement, Cement Concr. Res. 25 (1995) 561–571.
[70] S. Zhang, A. Keulen, K. Arbi, G. Ye, Waste glass as partial mineral precursor in alkali-activated slag/fly ash system, Cement Concr. Res. 102 (2017) 29–40, https://doi.org/10.1016/j.cemconres.2017.08.012.
[71] A. Favier, J. Hot, G. Habert, N. Roussel, J.B. D'Espinose De Lacaillerie, Flow properties of MK-based geopolymer pastes. A comparative study with standard Portland cement pastes, Soft Matter 10 (2014) 1134–1141, https://doi.org/10.1039/c3sm51889b.
[72] N. Roussel, G. Ovarlez, S. Garrault, C. Brumaud, The origins of thixotropy of fresh cement pastes, Cement Concr. Res. 42 (2012) 148–157, https://doi.org/10.1016/j.cemconres.2011.09.004.
[73] Y. Sun, S. Zhang, A.V. Rahul, Y. Tao, F. Van Bockstaele, K. Dewettinck, G. Ye, G. De Schutter, Rheology of alkali-activated slag pastes: new insight from microstructural

investigations by cryo-SEM, Cement Concr. Res. 157 (2022) 106806, https://doi.org/10.1016/j.cemconres.2022.106806.
[74] S.A. Bernal, J.L. Provis, R.J. Myers, R. San Nicolas, J.S.J. van Deventer, Role of carbonates in the chemical evolution of sodium carbonate-activated slag binders, Mater. Struct. Constr. 48 (2014) 517–529, https://doi.org/10.1617/s11527-014-0412-6.
[75] X. Dai, Q. Ren, S. Aydin, M.Y. Yardimci, G. De Schutter, Accelerating the reaction process of sodium carbonate-activated slag mixtures with the incorporation of a small addition of sodium hydroxide/sodium silicate, Cem. Concr. Compos. 141 (2023) 105118.
[76] N. Mikanovic, K. Khayat, M. Pagé, C. Jolicoeur, Aqueous CaCO3 dispersions as reference systems for early-age cementitious materials, Colloids Surfaces A Physicochem. Eng. Asp. 291 (2006) 202–211.
[77] M.H. Hubler, J.J. Thomas, H.M. Jennings, Influence of nucleation seeding on the hydration kinetics and compressive strength of alkali activated slag paste, Cement Concr. Res. 41 (2011) 842–846, https://doi.org/10.1016/j.cemconres.2011.04.002.
[78] B.S. Gebregziabiher, R. Thomas, S. Peethamparan, Very early-age reaction kinetics and microstructural development in alkali-activated slag, Cem. Concr. Compos. 55 (2015) 91–102, https://doi.org/10.1016/j.cemconcomp.2014.09.001.
[79] S.A. Bernal, R.S. Nicolas, J.S.J. van Deventer, J.L. Provis, Alkali-activated slag cements produced with a blended sodium carbonate/sodium silicate activator, Adv. Cement Res. 28 (2016) 262–273.
[80] B. Yuan, Q.L. Yu, H.J.H. Brouwers, Evaluation of slag characteristics on the reaction kinetics and mechanical properties of Na2CO3 activated slag, Construct. Build. Mater. 131 (2017) 334–346.
[81] Y. Zuo, G. Ye, Preliminary interpretation of the induction period in hydration of sodium hydroxide/silicate activated slag, Materials 13 (2020) 1–19, https://doi.org/10.3390/ma13214796.
[82] P. Duxson, J.L. Provis, Designing precursors for geopolymer cements, J. Am. Ceram. Soc. 91 (2008) 3864–3869, https://doi.org/10.1111/j.1551-2916.2008.02787.x.
[83] R. Cao, S. Zhang, N. Banthia, Y. Zhang, Z. Zhang, Interpreting the early-age reaction process of alkali-activated slag by using combined embedded ultrasonic measurement, thermal analysis, XRD, FTIR and SEM, Composites, Part B 186 (2020) 107840, https://doi.org/10.1016/j.compositesb.2020.107840.
[84] F. Puertas, A. Fernández-Jiménez, M.T. Blanco-Varela, Pore solution in alkali-activated slag cement pastes. Relation to the composition and structure of calcium silicate hydrate, Cement Concr. Res. 34 (2004) 139–148, https://doi.org/10.1016/S0008-8846(03)00254-0.
[85] D. Jiao, R. De Schryver, C. Shi, G. De Schutter, Thixotropic structural build-up of cement-based materials: a state-of-the-art review, Cem. Concr. Compos. 122 (2021) 104152.
[86] Y. Li, C. Yang, Y. Zhang, J. Zheng, H. Guo, M. Lu, Study on dispersion , adsorption and flow retaining behaviors of cement mortars with TPEG-type polyether kind polycarboxylate superplasticizers, Construct. Build. Mater. 64 (2014) 324–332, https://doi.org/10.1016/j.conbuildmat.2014.04.050.
[87] L. Kalina, V. Bílek Jr., R. Novotný, M. Mončeková, J. Másilko, J. Koplík, Effect of Na3PO4 on the hydration process of alkali-activated blast furnace slag, Materials 9 (2016) 395.
[88] X. Dai, S. Aydin, M.Y. Yardimci, G. De Schutter, Early structural build-up, setting behavior, reaction kinetics and microstructure of sodium silicate-activated slag mixtures with different retarder chemicals, Cement Concr. Res. 159 (2022) 106872.
[89] N. Garg, C.E. White, Mechanism of zinc oxide retardation in alkali-activated materials: an in situ X-ray pair distribution function investigation, J. Mater. Chem. A 5 (2017) 11794–11804.
[90] J.-J. Chang, A study on the setting characteristics of sodium silicate-activated slag pastes, Cement Concr. Res. 33 (2003) 1005–1011.